Geophysical Research Letters

RESEARCH LETTER
10.1029/2022GL097770

Key Points:

- The electron precipitation signature induced by a superbolt lightning event is modeled, which agrees with previous spacecraft observation
- The precipitation is decomposed into contributions from different wave frequency components and resonance modes to study its structure
- The spatiotemporal signature of global precipitation is analyzed. The total precipitation energy is >100x stronger than typical lightning

Supporting Information:

Supporting Information may be found in the online version of this article.

Correspondence to:

N. Kang,
nkang20@atmos.ucla.edu

Citation:

Kang, N., & Bortnik, J. (2022). Structure of energy precipitation induced by superbolt-lightning generated whistler waves. *Geophysical Research Letters*, *49*, e2022GL097770. https://doi.org/10.1029/2022GL097770

Received 6 JAN 2022
Accepted 10 FEB 2022

Author Contributions:

Conceptualization: Jacob Bortnik
Formal analysis: Ning Kang, Jacob Bortnik
Funding acquisition: Jacob Bortnik
Investigation: Ning Kang, Jacob Bortnik
Methodology: Ning Kang
Project Administration: Jacob Bortnik
Supervision: Jacob Bortnik
Visualization: Ning Kang
Writing – original draft: Ning Kang
Writing – review & editing: Ning Kang, Jacob Bortnik

Structure of Energy Precipitation Induced by Superbolt-Lightning Generated Whistler Waves

Ning Kang[1] **and Jacob Bortnik**[1]

[1]Department of Atmospheric and Oceanic Sciences, University of California, Los Angeles, CA, USA

Abstract Lightning superbolts are unusually intense lightning strokes. It has been well known that lightning can induce electron precipitation through the whistler waves it generates, but the characteristic of such precipitation in the extreme case of a superbolt has not yet been investigated. In this work, we use the numerical method developed by Bortnik et al. (2006a, https://doi.org/10.1029/2005ja011182, 2006b, https://doi.org/10.1029/2005ja011398) to model the precipitation induced by a superbolt event reported by Ripoll et al. (2021, https://doi.org/10.1038/s41467021237406). The modeled frequency spectrum agrees well with in situ measurements, adding confidence to the model performance. The precipitation flux is decomposed into contributions from different frequency components and different resonance types, thus revealing the underlying structure of the precipitation. The temporal signature of global precipitation on the ground surface is produced for potential comparison with observations by upcoming satellite missions.

Plain Language Summary Lightning superbolts are unusually intense lightning strokes. Previous studies have shown that lightning can emit electromagnetic radiation called whistler waves into space, which can interact with electrons and make electrons crash and be lost into the dense upper atmosphere. However, previous studies on this topic focus on typical intensity lightning, and what would happen during a superbolt is still unknown. In this work, we use a numerical method to simulate how the electrons would be lost into the atmosphere during one well studied superbolt event. Our simulated wave signal agrees well with the real in situ satellite observation, indicating that our simulation is reliable. We model the energy spectrum evolution of the energy flux, and we identify the electron loss contributed by different frequency electromagnetic radiation through different ways of interaction with electrons thus revealing the detailed structure of the precipitation signature. In that way the inner structure of this energy spectrum evolution and its various drivers can be understood. We also show in a short period after the superbolt, which part of the Earth surface will get hit by these falling electrons.

1. Introduction

Lightning superbolts are rare lightning strokes with unusually intense current and power, which were first observed by Turman (1977) using optical sensors aboard the Vela satellite. Recent statistical work based on the World Wide Lightning Location Network shows that superbolts are most likely to occur during northern hemisphere winter, in the North Atlantic west of Europe and in Mediterranean Sea (Holzworth et al., 2019). Superbolts also differ from typical lightning strokes in many aspects. Superbolts have a more symmetric ground wave peak due to a longer rise time; their power decays slower with distance in space compared to typical lightning and the power spectrum of superbolts is mainly confined to the very low frequency (VLF) range (Ripoll et al., 2021).

Lightning strokes emit electromagnetic power into the ionosphere (Crary, 1961), part of which then propagates through the ionosphere and couples into the whistler mode, bouncing back and forth in the magnetosphere (Kimura, 1966). These waves are called magnetospherically reflecting (MR) whistlers, and were first identified by the OGO1 and OGO3 satellites (Smith & Angerami, 1968). They are named 'whistler' waves because of the unique frequency chirping made due to its dispersion relation, which sounds like audible whistling tones when played through a loudspeaker (Storey, 1953). It has been extensively investigated and widely accepted that such lightning generated whistlers can induce pitch angle scattering and, consequently, electron precipitation, which is one of the important mechanisms for the loss of energetic particles in the radiation belt (Bell, 1984; Blake et al., 2001; Bortnik et al., 2002; 2006a, 2006b; Johnson, 1999; Peter & Inan, 2004).

However, the studies on the precipitation induced by whistlers have so far been limited to whistlers generated by typical lightning strokes. The precipitation signature induced by superbolt-generated whistlers looks is still

unclear. Also, the underlying structure of the precipitation signature and related physical processes have not been fully discussed. In this work, we seek to model the precipitation signature induced by a well studied recent superbolt event, and explore and understand its underlying structures. Our results could also provide a convenient theoretical reference for future observation works on precipitation by superbolt events.

2. Model and Method

We set up our model based on one of the superbolt events reported by Ripoll et al. (2021). The superbolt occurred at UTC 17:43:55, 23 January 2013, at around 42°N, 19°E near Montenegro. The local time is ∼7p.m., and is thus on the nightside. The peak current of the superbolt reached values as high as −326 kA. The RBSP-B spacecraft, located at $L = 2.43$, $MLT = 21.47$, $MLAT = 15°$, observed the whistler signals over the frequency range ∼100–10,000 Hz 0.5 s later.

The precipitation model we use is the model of Bortnik et al. (2006a, 2006b), which presents the technical aspect in great detail. Here we briefly summarize how this model calculates the precipitation flux due to a lightning stroke.

1. A cloud-to-ground lightning stroke emits waves with a wide range of frequencies from a range of latitudes around the lightning at the bottom of ionosphere. We then do ray tracing for the "sampled" rays launched from different latitudes λ_i with different frequencies f_j. The initial power of each ray, depending on their frequency and distance to the lightning, is given by a formula following Uman (1984, p. 61)
2. The "sampled" rays with adjacent frequencies (f_j and f_{j+1}) and source latitudes (λ_i and λ_{i+1}) can be interpolated to provide information for any arbitrary ray $[\lambda, f]$ with $\lambda_i < \lambda < \lambda_{i+1}$ and $f_j < f < f_{j+1}$ using linear interpolation. This interpolation technique enables us to obtain ∼120 million rays whilst actually running only ∼5,000 ray tracing runs, which saves computation time tremendously
3. We then set multiple "observation points" over different latitudes on the field line of interest at a given L shell. Each sampled or interpolated ray is examined whether it went through one of the observation points, and if so, the ray power is added to the appropriate bin of frequency-time (f-t) spectrum of that observation point
4. After the f-t spectrum is obtained for all observation points on the field line, the pitch angle change $\Delta\alpha$ due to scattering by each f-t bin of each observation point is calculated based on Bell (1984, Equation 47), which is added to the resonance energy – time (E-t) bin of this L shell (where the time correction due to the flight time from observation point to the foot point is also considered)
5. Combined with appropriate equatorial trapped flux model (e.g., AE8 model (Vette, 1991)), using a convolutional approach (Bortnik et al., 2006a, Figure 10 and Equation. 18), the pitch angle change in each E-t bin can be converted to a precipitation flux. This leads us to our desired E-t spectrum of precipitation flux for a specific L shell

In this work, we set 41 source latitudes ±10° around the superbolt, that is, 32°–52°. There are in total 150 frequency components ranging 200–60,000 Hz evenly spaced in log scale. This gives us in total 6,150 "sampled" rays. 200 source latitudes/frequencies are linearly interpolated between adjacent source latitudes/frequencies, which gives us 246 million "interpolated" rays. We calculate the precipitation flux for 23 L shells ranging from 1.22 to 4.85, whose invariant latitudes are evenly spaced between 25° and 63°. The ionospheric attenuation factor is obtained based on the data from Helliwell (1965, Figures 3–35) similar to Bortnik et al. (2003). Because the superbolt event occurred on the night side, we use the nightside data, which gives a significantly lower attenuation factor than the dayside data, and corresponds to the region where most lightning-generated whistlers are observed in space (Green et al., 2020). Note that the Helliwell curve is quite accurate at such higher latitude of 40° on the night side, compared to more recent full wave model results (Tao et al., 2010).

3. Results and Discussion

3.1. Frequency Spectrum

Figure 1 shows the whistler wave signature characteristic for the observation point at $L = 2.4$, $MLAT = -15°$, which is set to the L shell and latitude of RBSP-B during the observed superbolt event. Figure 1b is the *f-t* spectrum between ∼100 and 10,000 Hz for the first 5 s following the lightning strike. We observe 6 clear elements, whose locations and shapes match very well with observed in situ measurements by RBSP-B (compare with

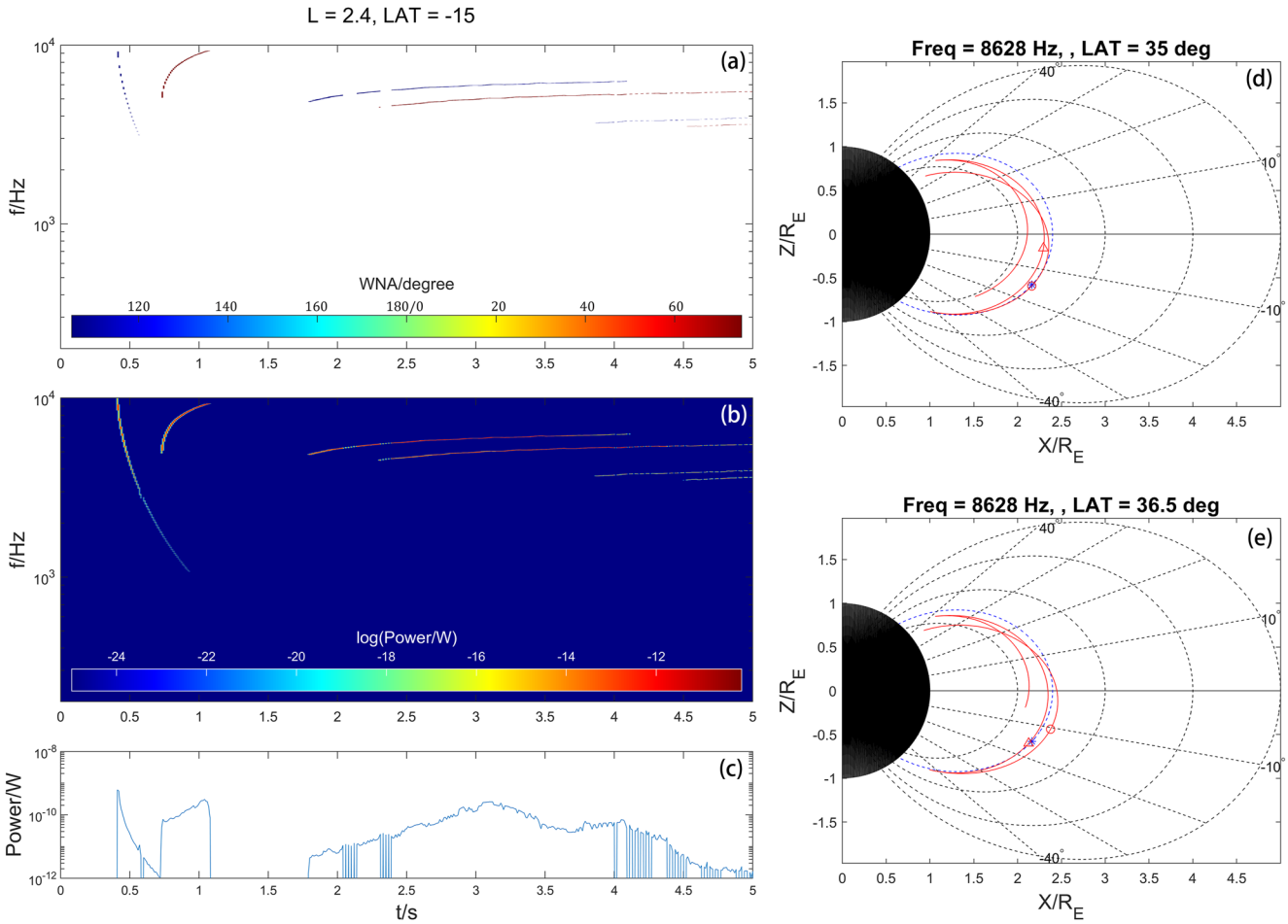

Figure 1. (a) Averaged wave normal angle frequency-time spectrum. (b) Wave power frequency-time spectrum. (c) Total wave power evolution. (d), (e) are example of rays with the same frequency crossing the observation point from different direction. The red solid lines are ray trajectories, black dashed lines are reference lines for field lines and different latitudes, blue dashed line is the reference line for $L = 2.4$ where the observation point locates, and the blue asterisk is the location of the observation point. The red circle and triangle markers are the ray location at 0.43 and 0.91 s, respectively. Ray in (d) is launched from latitude 35°, and ray in (e) from 36.5°.

Figure 3a, Ripoll et al., 2021). Integrating over all frequency components of the *f*-*t* spectrum, we obtain the total wave power evolution as shown in Figure 1c. The wave power evolution also matches very well with in situ measurement (compare with Figures 3b Ripoll et al., 2021), reproducing the two peaks at ∼0.5 and ∼0.8 s with similar magnitudes and the power plateau arising at around 1.8 s with a magnitude lower than the previous two peaks. The good agreement between our simulated *f*-*t* spectrum and in situ measurement indicates that our model well captures the physical processes leading to this observation. Some slight differences like the not-completely-similar shapes of spectrum elements might be due to a 3-hr MLT difference between the superbolt event (and thus the meridional plane where the ray tracing is conducted) and the RBSP-B spacecraft. Although our chosen observation point has the same *L* shell and latitude as the spacecraft, they are separated on the longitudinal direction, which may contribute some minor observed differences.

Ripoll et al. notes the similarity between the two peaks in the first second. They propose the second peak is made up by waves consisting of the first peak, but slightly different in source latitude, so that they undergo a magnetospheric reflection and cross the spacecraft from the opposite direction ∼0.2 s later. Our results provide a strong theoretical support to this claim. Figure 1a shows the averaged wave normal angle (WNA) corresponding to the whistler in Figure 1b. We see that the first two elements have opposite WNA directions. The first element has a WNA >90°, indicating southward propagating waves, while the second has a WNA <90°, indicating northward propagating waves (the Poynting vector always has the same direction as the WNA for a whistler wave). For a specific example of two ray trajectories please see Figures 1d and 1e, where the blue asterisk is the observation

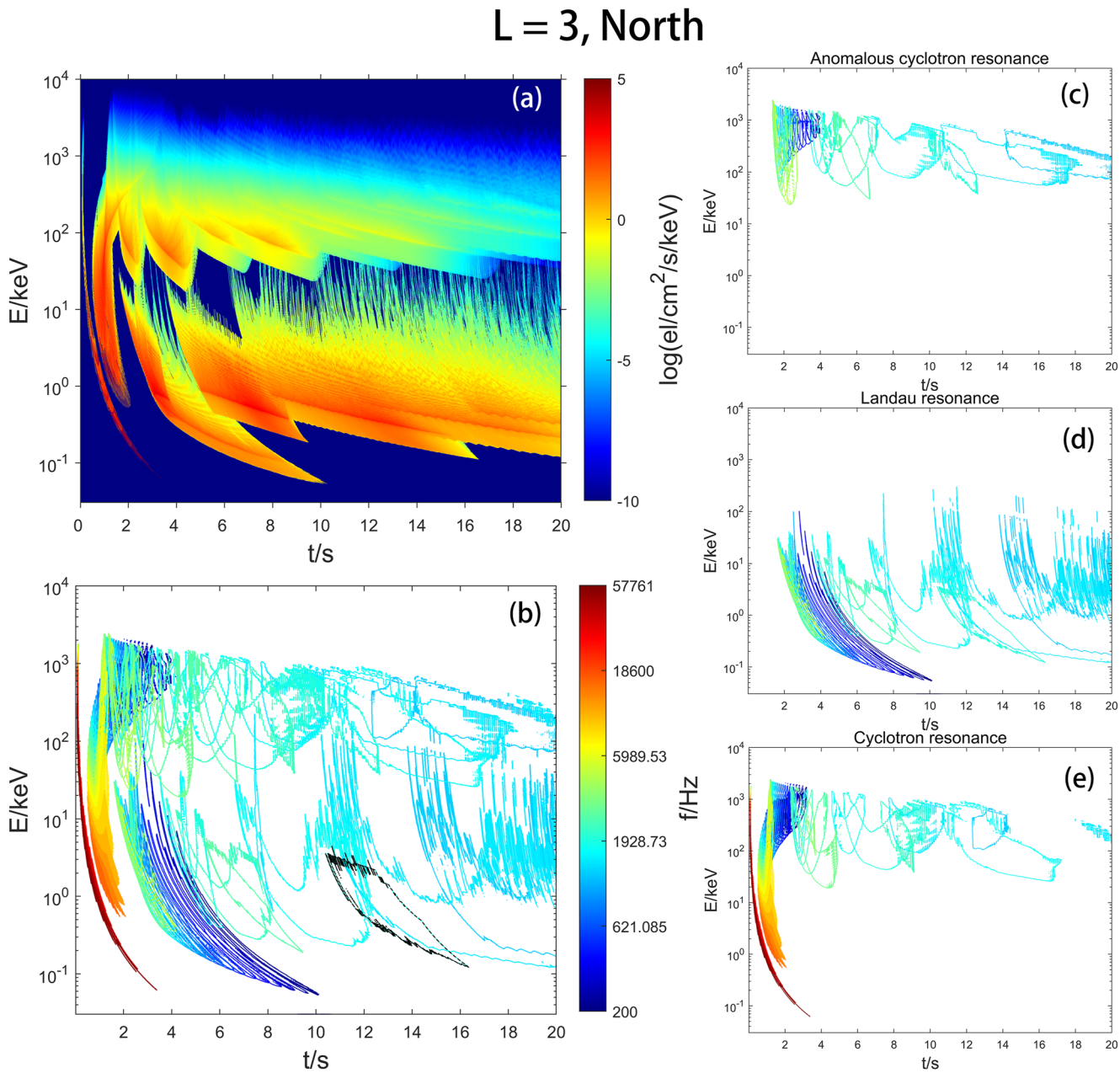

Figure 2. (a) Energy-time spectrum of precipitation flux on northern hemisphere on L shell of 3. (b) Precipitation energy flux energy-time spectrum decomposed into contribution from different energy. Each contour marks a region with significant precipitation flux contributed by a specific frequency component, which is marked by the contour color. One such contour (from the frequency component of 2034 Hz) is overlaid by the black dashed line for illustrative purpose. (c)∼(e) are the same as subplot (b), but include contribution from resonance with harmonic mode of −1 (anomalous cyclotron), 0 (Landau) and 1 (cyclotron) only, respectively.

point, the red circle and triangle markers are the ray location at 0.43 and 0.91 s, respectively. It's clear that the 8,628 Hz ray passed through the observation point southward at 0.43s if it is launched from a latitude 35°, but northward at 0.91s after bouncing back if it is launched from a latitude 36.5°, consistent with observations.

3.2. Structure of the Precipitation Spectrum

Figure 2 shows the precipitation energy flux spectrum observed in the Northern hemisphere footpoint at an L-shell of 3. Figure 2a is the precipitation energy flux Q, which resembles the results in Bortnik et al. (2006a), except that the flux in this work is ∼2–3 orders of magnitude stronger than Bortnik et al. (2006a) due to the

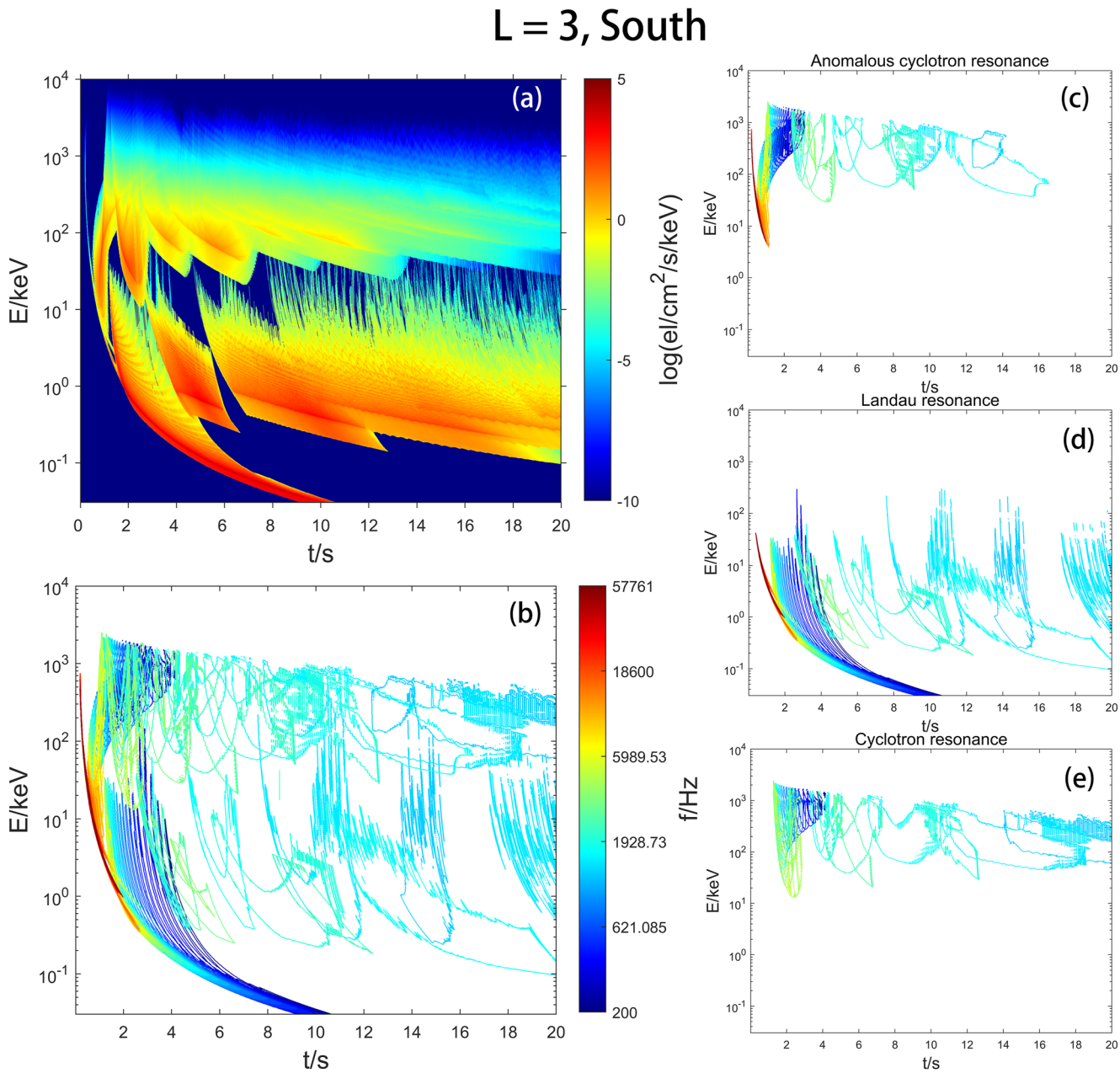

Figure 3. The same as Figure 2 but for precipitation flux on southern hemisphere on L shell of 3.

much higher lightning power. In this work, we focus on analyzing the underlying structure of this precipitation flux spectrum, including the contribution from different frequency components and different resonance modes. For this we use a new visualization method to illustrate the precipitation flux in Figure 2a. The precipitation flux contributed by each frequency component is outlined by a $Q = 1 \times 10^{-6}\ cm^{-2}s^{-1}\ keV^{-1}$ contour line, and the frequency is represented by the color of the contour line. As an example, for the green contour marked by an overlaid black dashed line in Figure 2b, the green color means this part of precipitation flux is driven by the frequency component of $f = 2034$ Hz waves (as inferred from the color bar), and the area enclosed by the contour has a precipitation flux greater than $1 \times 10^{-6}\ cm^{-2}s^{-1}\ keV^{-1}$. Putting all such contours together into one figure, we have Figure 2b, which clearly decomposes Figure 2a into contributions from whistler waves with different frequency components.

Figure 2b shows that the highest frequency components (>10 kHz) only contribute to the precipitation for just the first few seconds. This is because rays with high frequencies cannot undergo a magnetospheric reflection, but quickly impinge upon the ionosphere and get absorbed, as well as getting Landau damped very quickly (usually within 1 s). Therefore, they don't have a chance to produce long-term precipitation. The lowest frequency components (<1 kHz) also contribute to only the first few seconds at $L = 3$, but the underlying physics limiting their contribution is different. The low frequency waves get damped much slower so they can endure for a very long time, but they also propagate outward to the outer L shells quickly. Therefore, for a lower L shell of interest like three in this case, the low frequency waves will cross it only once at an early stage. Only the middle frequency components around 2 kHz can both survive a sufficiently long time while bouncing back and forth around the L shell of interest and crossing it repeatedly (since the wave frequency is comparable to the lower hybrid resonance frequency), therefore producing precipitation lasting over 10 s, as seen in Figure 2b after 6 s. For a specific example of the typical ray behavior for the high, middle and low frequency rays, please see Figure S1 in Supporting Information S1.

To further understand the precipitation structure, we further decompose Figure 2b according to contributions by different resonance harmonic number M_{res}. Figures 2c–2e are the same as Figure 2b but only include precipitation flux caused by anomalous cyclotron resonance ($M_{res} = -1$), Landau resonance ($M_{res} = 0$) and normal (counter-streaming) cyclotron resonance ($M_{res} = 1$), respectively. They share the same color bar as Figure 2b. We now clearly see that the highest frequency components contribute to precipitation flux only through normal cyclotron resonance. This is because, as discussed earlier, the high frequency rays don't experience bouncing, thus can cross the L shell of interest in only one direction. Because the superbolt occurs on the northern hemisphere, the emitted waves can cross L shell of three only in the southward direction. For electrons precipitating into northern hemisphere, they are counter-stream particles, therefore are limited to the normal cyclotron resonance interaction. Another interesting feature to be noted is that the precipitation due to Landau resonance usually has a much lower energy than (anomalous) cyclotron resonance. The lowest frequency components, in particular, contribute the lowest energy precipitation through Landau resonant interaction, as indicated in Figure 2d around $t = 10s$.

Figure 3 is presented in the same format as Figure 2, but is for precipitation to the southern hemisphere footpoint of $L = 3$. The results and conclusions are similar to the northward precipitation except for two interesting differences. The first is that although the highest frequency components still contribute to only the first few seconds of the precipitation signature, they are now produced via Landau and anomalous cyclotron resonance, as shown in Figures 3c and 3d. This can be easily understood if one notices that for southward precipitating electrons, they are now co-streaming particles with respect to the high frequency waves (which cross L shell of three only southward as mentioned earlier), therefore only Landau and anomalous cyclotron resonance are possible instead of normal (counter-streaming) cyclotron resonance. Another interesting difference is that the precipitation induced by the lowest frequency waves through Landau resonance has even lower energies than those in the northern hemisphere. The underlying physics is also understandable if one notices that the waves are all initially southward propagating, therefore to allow northward-moving electrons to undergo Landau resonance, they must interact with northward propagating waves, which must have encountered a bouncing to change the propagating direction, during which the waves will become significantly more oblique, thus having a smaller parallel wave number $k_{\parallel}$ and, consequently, a higher Landau resonance energy. The southward-moving electrons, on the other hand, can directly undergo Landau resonance with waves that have not yet experienced MR bouncing, whose $k_{\parallel}$ then still remain large, leading to a lower Landau resonance energy.

3.3. Global Precipitation Signature

The total precipitated energy flux evolution on one single L shell can be easily calculated by integrating the flux spectrum over energy. By combining the fluxes from multiple L shells (corresponding to multiple invariant latitudes), a total precipitation energy flux evolution over latitudes can be obtained. However, to give the total energy flux distribution at 100 km altitude, an additional assumption is needed to extrapolate the flux in the longitudinal direction. Here we follow the method of Bortnik (2004) and Bortnik et al. (2006b), which proposes that the precipitation flux ratio for ground location off and on the longitude of the lightning can be described by the square root of the initial wave power ratio, which is described by Uman (1984, p. 61). This gives us the scaling function:

$$s(\lambda,\phi) \equiv \frac{Q(\lambda,\phi)}{Q(\lambda,\phi_0)} = \frac{R(\lambda,\phi_0)\sin\theta(\lambda,\phi)}{R(\lambda,\phi)\sin\theta(\lambda,\phi_0)}, \quad (1)$$

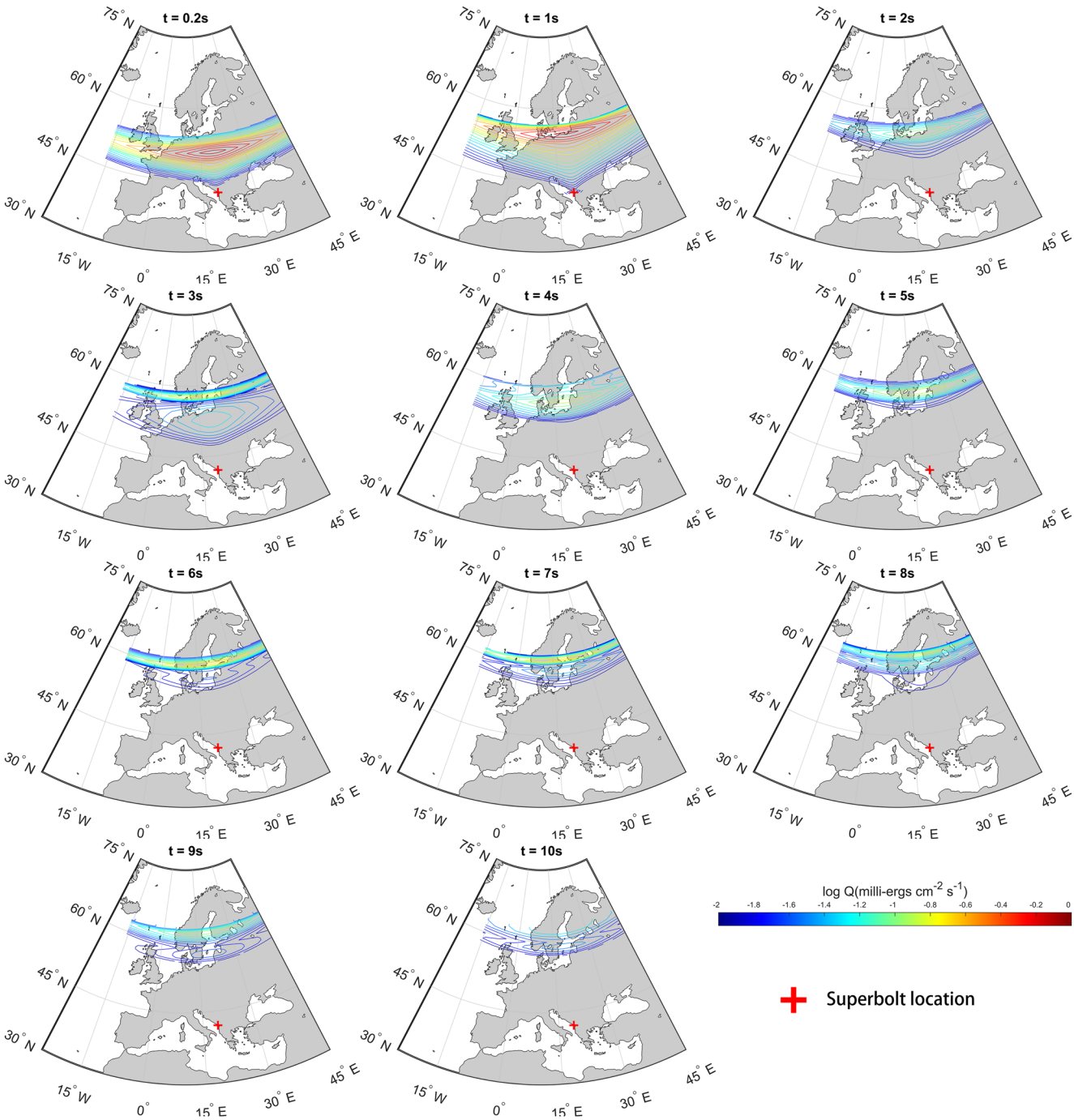

Figure 4. Global precipitation signature for the first 10 s after the superbolt event. The gray area is the land, the red cross is the superbolt location, and the colored contour is the spatial distribution of precipitation energy flux.

where λ, ϕ are the latitude and longitude of an arbitrary ground location, ϕ_0 is the longitude of the superbolt, R (λ, ϕ) and $\theta(\lambda, \phi)$ are the distance and zenith angle of location (λ, ϕ) with respect to the superbolt location. Because Q (λ, ϕ_0) can be easily obtained, by calculating the scaling function s (λ, ϕ) we obtain the total precipitation energy flux evolution at the assumed precipitation altitude of 100 km.

Figure 4 shows the spatiotemporal signature of the superbolt lightning-induced electron precipitation (for a video demonstration please refer to Supporting Information S1). The red cross marks the superbolt location, and the contours show the total energy flux. We see that the precipitation all occurs on higher latitudes than the superbolt

because the resulting whistler waves propagate to higher L shells, which correspond to higher invariant latitudes on the ground. This also explains why the precipitation center keeps moving northward. Interestingly the velocity of the precipitation center decreases dramatically. In the first second the averaged velocity of the precipitation center is about 521 km/s, but in the second second the precipitation center hardly moves at all. New precipitation center keeps forming on the south (e.g., at 3, 6 and 9 s) due to the MR bouncing of the whistler wave packet in space, thus forming a banded precipitation structure. Compared with the results of Bortnik (2004), and Bortnik et al. (2006a, 2006b) the total precipitation flux induced by a superbolt is 2–3 order of magnitude stronger, which is also a consequence of the extremely high power of superbolt.

4. Conclusion

Here, we modeled the electron precipitation flux induced by a superbolt lightning event that occurred at UTC 17:43:55, 23 January 2013 using observed parameters in a recently published study by Ripoll et al. (2021). The modeled frequency-time spectrum of emitted whistlers agrees well with the simultaneous RBSP-B observations. The precipitation energy flux spectrum is similar to that of typical lightning except that the flux is a factor of 2–3 stronger. The structure of the induced precipitation flux spectrum is analyzed using a new decomposition method. It was shown that both the low frequency (<1 kHz) and high frequency (>10 kHz) wave components only contribute to the first few seconds of the electron precipitation at $L = 3$, while the middle frequency (~ 2 kHz) wave components contribute to prolonged precipitation. This is because high frequency components cannot bounce back and get Landau damped quickly, and the low frequency components propagate to the outer L shell quickly so they cross the lower L shells only once. Only the middle frequency components have both a moderate damping rate, and repeatedly bounce around the lower L shell of interest, if the wave frequency is close to the equatorial lower hybrid resonance frequency. The high energy (>10 keV) electron precipitation is mainly contributed by normal and anomalous cyclotron resonance, while the low energy (<10 keV) precipitation is predominantly contributed by Landau resonance. In particular, the lowest energy precipitation is contributed by lowest frequency components through Landau resonance, and the southern hemisphere has lower minimum precipitation energies than northern hemisphere because waves originated from northern hemisphere can have Landau resonance with only southward moving electrons before encountering a bounce.

The time evolution of the precipitation flux signature on ground surface is calculated. The precipitation occurs predominantly north of the superbolt location, and the precipitation center moves northward with a very high velocity. The precipitation pattern exhibits a latitudinally banded structure because new precipitation centers keep forming south of old precipitation centers. The total precipitation energy is about ~2–3 times stronger than those induced by typical lightning. This work provides a direct prediction of a superbolt (as well as intense) lightning-generated electron precipitation signatures that can be directly compared to observations by recently launched (e.g., ELFIN mission (Angelopoulos et al., 2020)) and upcoming CubeSat missions designed to observe electron precipitation, and helps to deepen our understanding of the mechanism and structure of lightning-induced electron precipitation.

Data Availability Statement

The data can be accessed from https://doi.org/10.5281/zenodo.5826319.

Acknowledgments
NK and JB gratefully acknowledge NASA FINESST award 80NSSC21K1393 and NSF Geospace Environment Modeling Grant No. AGS-2025706.

References

Angelopoulos, V., Tsai, E., Bingley, L., Shaffer, C., Turner, D. L., Runov, A., et al. (2020). The ELFIN mission. *Space Science Reviews*, *2165*, 1–45.

Bell, T. F. (1984). The nonlinear gyroresonance interaction between energetic electrons and coherent VLF waves propagating at an arbitrary angle with respect to the Earth's magnetic field. *Journal of Geophysical Research: Space Physics*, *89*, 905–918. https://doi.org/10.1029/ja089ia02p00905

Blake, J. B. (2001). Lightning-induced energetic electron flux enhancements in the drift loss cone. *Journal of Geophysical Research: Space Physics*, *106*, 29733–29744. https://doi.org/10.1029/2001ja000067

Bortnik, J. (2004). *Precipitation of radiation belt electrons by lightning-generated magnetospherically reflecting whistler waves*. Stanford university.

Bortnik, J., Inan, U. S., & Bell, T. F. (2002). L dependence of energetic electron precipitation driven by magnetospherically reflecting whistler waves. *Journal of Geophysical Research: Space Physics*, *107*. https://doi.org/10.1029/2001ja000303

Bortnik, J., Inan, U. S., & Bell, T. F. (2003). Frequency-time spectra of magnetospherically reflecting whistlers in the plasmasphere. *Journal of Geophysical Research*, *108*(A1), 1030. https://doi.org/10.1029/2002JA009387

Bortnik, J., Inan, U. S., & Bell, T. F. (2006a). Temporal signatures of radiation belt electron precipitation induced by lightning-generated MR whistler waves: 1. Methodology. *Journal of Geophysical Research: Space Physics*, *111*. https://doi.org/10.1029/2005ja011182

Bortnik, J., Inan, U. S., & Bell, T. F. (2006b). Temporal signatures of radiation belt electron precipitation induced by lightning-generated MR Whistler waves: 2. Global signatures. *Journal of Geophysical Research*, *111*, A02205. https://doi.org/10.1029/2005JA011398

Crary, J. H. (1961). *The effect of the Earth-ionosphere waveguide on whistlers*. STANFORD UNIV CA STANFORD ELECTRONICS LABS.

Green, A., Li, W., Ma, Q., Shen, X. C., Bortnik, J., & Hospodarsky, G. B. (2020). Properties of lightning generated whistlers based on Van Allen Probes observations and their global effects on radiation belt electron loss. *Geophysical Research Letters*, *47*, e2020GL089584. https://doi.org/10.1029/2020GL089584

Helliwell, R. A. (1965). *Whistlers and Related Ionospheric Phenomena* (Vol. 50). Stanford University Press.

Holzworth, R. H., McCarthy, M. P., Brundell, J. B., Jacobson, A. R., Rodger, C. J. (2019). Global distribution of superbolts. *Journal of Geophysical Research: Atmospheres*, *24*, 9996–10005. https://doi.org/10.1029/2019jd030975

Johnson, M. P. (1999). VLF imaging of precipitation of energetic electrons by oblique whistlers. *Geophysical Research Letters*, *26*, 3569–3572. https://doi.org/10.1029/1999gl010706

Kimura, I. (1966). Effects of ions on whistler-mode ray tracing. *Radio Science*, *13*, 269–283. https://doi.org/10.1002/rds196613269

Peter, W. B., & Inan, U. S. (2004). On the occurrence and spatial extent of electron precipitation induced by oblique nonducted whistler waves. *Journal of Geophysical Research: Space Physics*, *109*. https://doi.org/10.1029/2004ja010412

Ripoll, J. F., Farges, T., Malaspina, D. M., Cunningham, G. S., Lay, E. H., Hospodarsky, G. B., et al. (2021). Electromagnetic power of lightning superbolts from Earth to space. *Nature Communications*, *121*, 1–10. https://doi.org/10.1038/s41467-021-23740-6

Smith, R. L., & Angerami, J. J. (1968). Magnetospheric properties deduced from OGO 1 observations of ducted and nonducted whistlers. *Journal of Geophysical Research*, *731*, 1–20. https://doi.org/10.1029/ja073i001p00001

Storey, L. R. O. (1953). An investigation of whistling atmospherics. *Philosophical Transactions of the Royal Society*, *246*.

Tao, X., Bortnik, J., & Martin, F. (2010). Variance of transionospheric VLF wave power absorption. *Journal of Geophysical Research: Space Physics*, *115*. https://doi.org/10.1029/2009ja015115

Turman, B. N. (1977). Detection of lightning superbolts. *Journal of Geophysical Research*, *8218*, 2566–2568. https://doi.org/10.1029/jc082i018p02566

Uman, M. A. (1984). *Lightning* (reprint ed., pp. 3–573).

Vette, J. I. (1991). *National Aeronautics and Space Administration* (Vol. 91). National Space Science Data CenterGoddard Space Flight Center. The AE-8 trapped electron model environmentNo. 24(NSSDC), World Data Center A for Rockets and Satellites (WDC-AR & S).